Visible-light-driven Photocatalytic Degradation of Erythrosine using Carbon-doped SnO_2 Quantum Dots

Dinesh Bourasi[1]*, Jayesh Bhatt[2], Seema Kothari[3*]

Abstract

Persistent organic pollutants, particularly synthetic dyes, pose a significant environmental challenge due to their chemical stability, resistance to biodegradation, and potential toxicity. Conventional wastewater treatment methods often fail to achieve complete removal of such contaminants, necessitating the development of more efficient and sustainable approaches. In the present study, carbon-doped SnO_2 quantum dots were synthesized via a hydrothermal method and evaluated as photocatalysts for the visible-light-driven degradation of erythrosine. The synthesized materials were characterized using X-ray diffraction, Fourier transform infrared spectroscopy, field emission scanning electron microscopy, energy dispersive spectroscopy, high-resolution transmission electron microscopy, and UV–visible spectroscopy, confirming the formation of SnO_2 quantum dots with successful carbon incorporation and reduced band gap. Photocatalytic activity was assessed by monitoring the degradation of erythrosine under visible-light irradiation, and the influence of key operational parameters, including solution pH, dye concentration, catalyst loading, and light intensity, was systematically investigated. The results demonstrated that the degradation process follows pseudo-first-order kinetics and is strongly dependent on experimental conditions, with optimal performance observed under near-neutral pH and specific catalyst and light intensity ranges. Carbon doping significantly enhanced the photocatalytic efficiency compared to undoped SnO_2 QDs, which is attributed to improved light absorption and charge carrier dynamics. A tentative mechanism involving reactive oxygen species, particularly hydroxyl radicals, is proposed based on experimental observations. These findings highlight the potential of carbon-doped SnO_2 quantum dots as effective photocatalysts for dye degradation under visible light and provide insights into the optimisation of photocatalytic processes for wastewater treatment applications.

Keywords: Carbon-doped SnO_2; Quantum dots; Photocatalytic degradation; Erythrosine; Visible light photocatalysis; Reaction kinetics

[1,2,3]Department of chemistry, Pacific Academy of Higher Education and Research University. Udaipur, 313003 (Rajasthan), INDIA *dns165br@gmail.com
*Corresponding author

Introduction

Persistent organic pollutants (POPs), particularly synthetic dyes, represent a major class of contaminants in aquatic environments due to their widespread industrial use and environmental persistence (1-4). These compounds are extensively discharged from textile, pharmaceutical, and food processing industries, often entering water bodies without complete treatment (3,5,6). Their complex aromatic structures confer high chemical stability and resistance to biodegradation, allowing them to persist in the environment over extended periods (7,8). In addition to their persistence, many synthetic dyes exhibit toxic, mutagenic, and carcinogenic effects, posing risks to both aquatic organisms and human health (4,6). The presence of dyes in water systems has significant ecological consequences. Even at low concentrations, these compounds impart intense colour to water, reduce light penetration, and disrupt photosynthetic activity in aquatic ecosystems (3,5). This reduction in light availability can alter dissolved oxygen levels and affect the survival of aquatic flora and fauna (3,8). Consequently, the removal of such pollutants from wastewater has become an important environmental and public health priority, necessitating the development of efficient and sustainable treatment strategies (7,9).

Conventional wastewater treatment approaches, including adsorption, coagulation, and biological degradation, are widely employed for dye removal; however, these methods often result in incomplete removal or transfer of pollutants rather than complete mineralization (3,4,5,9,10). In particular, adsorption and coagulation can generate secondary waste streams requiring further handling, while biological processes are limited by the recalcitrant nature of many synthetic dyes and their resistance to enzymatic breakdown (6-8,11). These limitations have driven the development of advanced treatment strategies capable of achieving more effective degradation. Photocatalysis has emerged as a promising alternative, relying on semiconductor materials to generate reactive oxygen species under light irradiation, which can oxidize organic pollutants into less harmful or fully mineralized products (3,12,13). This approach has been widely investigated within the broader framework of advanced oxidation processes, which aim to exploit highly reactive radical species for pollutant degradation (4,14). Despite its potential, commonly used photocatalysts such as TiO_2 and ZnO are restricted by their wide band gaps, limiting activation primarily to ultraviolet light, which constitutes only a small fraction of the solar spectrum (15,16). In addition, rapid electron–hole recombination in these materials reduces the efficiency of reactive species generation and constrains overall photocatalytic performance (7,17,18). These challenges have led to increasing efforts to develop modified photocatalytic systems with improved visible-light activity and enhanced charge carrier dynamics.

Tin dioxide (SnO_2) has been explored as an alternative photocatalyst due to its chemical stability, low toxicity, and strong oxidative potential (7). However, its practical application is limited by a wide band gap and inefficient charge carrier separation, which restrict its activity under visible-light irradiation (3). To address these limitations, nanoscale engineering and doping strategies have been widely investigated. The use of quantum dots provides a high surface-to-volume ratio, increased availability of active sites, and size-dependent electronic properties, which can enhance adsorption and photocatalytic reactivity (19-21). In parallel, non-metal doping has been shown to modify the electronic structure of semiconductor materials by introducing additional energy states, enabling band gap reduction and improved visible-light absorption (15,18,22). Carbon incorporation can also influence charge carrier dynamics by facilitating separation, acting as electron traps, and reducing recombination losses (23,24). The combination of these approaches, through the development of carbon-doped SnO_2 quantum dots, represents a strategy to enhance photocatalytic efficiency by simultaneously improving light absorption, surface reactivity, and charge carrier behavior.

Several studies have explored doped SnO_2 and related semiconductor systems for photocatalytic applications, although their scope remains fragmented. For instance, Rama Krishnappa and Lakshmipathi (25) investigated C-, N-, and S-doped SnO_2 systems and demonstrated enhanced photocatalytic activity through band-gap engineering, although the study primarily focused on electronic modification rather than systematic optimization of operational parameters. Similarly, Pan et al. (26) reported that defect engineering and oxygen vacancies can significantly alter photocatalytic behaviour through modified charge carrier dynamics, while Batzill and Diebold (27) highlighted the importance of surface properties and electronic structure in determining SnO_2 reactivity. Studies on doped TiO_2 systems, such as those by Asahi et al. (15) and Sakthivel and Kisch (18), established the role of non-metal doping in band-gap modification and visible-light activation, while subsequent work further demonstrated the importance of defect states and surface chemistry in photocatalytic performance (17,22). However, these studies do not directly address SnO_2-based quantum dot systems or parameter-driven optimization. In contrast, work on metal-doped SnO_2

quantum dots, such as Reddy et al. (28), has focused on dopant-specific electronic effects and charge transfer behaviour, with less attention to process-level variables.

Collectively, these studies highlight advances in material design but reveal a lack of integrated analysis linking photocatalytic performance, kinetic behaviour, and operational optimization under visible-light conditions, which the present study seeks to address. Despite increasing interest in doped semiconductor photocatalysts, there remains limited systematic evaluation of carbon-doped SnO_2 systems under visible-light conditions, particularly with respect to kinetic behaviour and the influence of operational parameters. Previous studies have often focused on material synthesis and basic performance assessment, with less emphasis on integrated optimization across variables such as pH, dye concentration, catalyst loading, and light intensity. As a result, a comprehensive understanding of how these factors collectively influence photocatalytic efficiency remains incomplete.

In this context, there is a need for an integrated investigation that combines material performance with process-level optimization. The present study aims to synthesize carbon-doped SnO_2 quantum dots and evaluate the photocatalytic degradation of erythrosine using carbon-doped SnO_2 quantum dots under visible-light irradiation. The study examines the degradation kinetics, investigates the effect of key operational parameters, compares performance with undoped SnO_2, and proposes a tentative degradation mechanism based on experimental observations. This approach is intended to provide a more comprehensive assessment of both material functionality and reaction behaviour.

Materials and Methods

Materials and Reagents

The tin precursor given to prepare SnO_2 quantum dots was tin(IV) chloride pentahydrate ($SnCl_4.5H_2O$). The carbon source used was glucose and urea was used as a precipitating and reaction-controlling agent. Erythrosine dye was employed as a model organic pollutant in the study to degrade photo catalytically. Synthesis and washing were done using deionized water and ethanol.

Synthesis of Carbon-Doped SnO_2 Quantum Dots

A modified hydrothermal method reported by Tirado-Guizar et al. was used to synthesize the Carbon-doped SnO_2 quantum dots (29). A 20 ml aqueous solution of 4 mmol. $SnCl_4 \cdot 5H_2O$ was first prepared under constant stirring. Another solution of 2 mmol of glucose was then made in 20 ml of deionized water and was added to the precursor solution and stirred to facilitate complete mixing. This was followed by a controlled addition of a 30 ml of 40 mmol urea solution while stirring continuously in the solution. The mixture was then transferred into a Teflon-lined stainless-steel autoclave and hydrothermal treatment of 90°C for 5 hrs. was performed. These were chosen so as to allow controlled nucleation and growth of particles at the nanoscale coupled with allowing effective incorporation of carbon within the SnO_2 matrix. After the hydrothermal reaction, the autoclave was left to cool to room temperature. The resulting precipitate was collected by centrifugation and washed five times with deionized water and two times with ethanol. The precipitate was dried at 60°C overnight. The resulting dry powder was then further heated at 400°C for 2 hrs. to enhance crystallinity and allow the SnO_2 quantum dot structure to form.

The Pure (undoped) SnO_2 quantum dots were prepared by an identical procedure using 20 ml of deionized water without glucose to maintain the same total volume.

Material Characterization

X-ray diffraction (XRD) patterns were recorded on a PANalytical, Netherlands, X'Pert Pro diffractometer using Cu Kα radiation (λ = 0.15406 nm). FESEM images and EDS/elemental mapping were obtained on a SU-8010 Series instrument (Hitachi, Japan). HRTEM images and SAED patterns were recorded on a JEOL, JEM-2100 Plus. XPS measurements were performed on a Thermo Fisher Scientific, K-ALPHA system. FTIR spectra were recorded on a Bruker ALPHA II spectrometer. UV-Vis diffuse reflectance spectra (DRS) were recorded on a PerkinElmer, USA, Lambda19 UV-VIS-NIR Spectrophotometer

Results and Discussion

Structural and Morphological Characterization of C-doped SnO_2 Quantum Dots

X-ray Diffraction (XRD) Analysis

The crystalline structure of the synthesized carbon-doped SnO_2 quantum dots was examined by the X-ray diffractometer (XRD) PANalytical X'Pert Pro using Cu Anode, Kα radiation (λ = 0.15406 nm) in the 2θ scanning ranges from 5° to 80°. Diffraction pattern (Figure 1) presents typical peaks of tetragonal rutile phase of SnO_2, which are in line with JCPDS data (No. 41-1445). The key reflections are marked to the (110), (101), (200) and (211) planes, which ensured the purity of the phases. The presence of a small peak shift as compared to bulk SnO_2 indicates a lattice distortion as a result of carbon incorporation.

The average crystallite size was estimated using the Debye–Scherrer equation:

$$D = (k\lambda/\beta \cos \theta)$$

where D is the mean crystallite size, K = 0.9 is the dimensionless shape factor, λ = 0.15406 nm is the X-ray wavelength (Cu Kα), β is the full-width at half-maximum (FWHM) of the diffraction peak in radians, and θ is the Bragg's angle. The mean size of crystallites obtained was about 3.2 nm, which is a sign of the creation of nanoscale quantum dots.

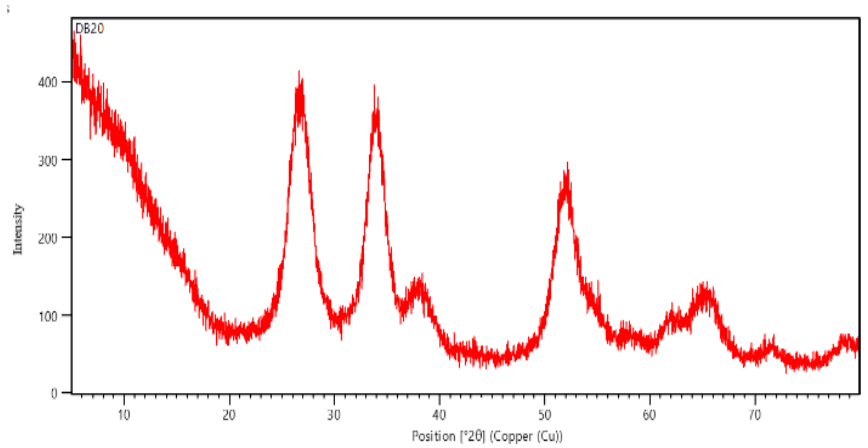

Figure 1. XRD pattern of carbon-doped SnO_2 quantum dots showing characteristic peaks of the rutile phase.

Field Emission Scanning Electron Microscopy (FESEM) Analysis

FESEM images of C-doped SnO_2 QDs recorded on Hitachi, SU-8010 Series was used to study the surface morphology shown in Fig. 2. As the images show, there are agglomerated nanostructures of fine crystalline particles with grain-like closely packed features. This structure is characteristic of hydrothermal nanomaterials syntheses, and can affect surface interactions in photocatalysis.

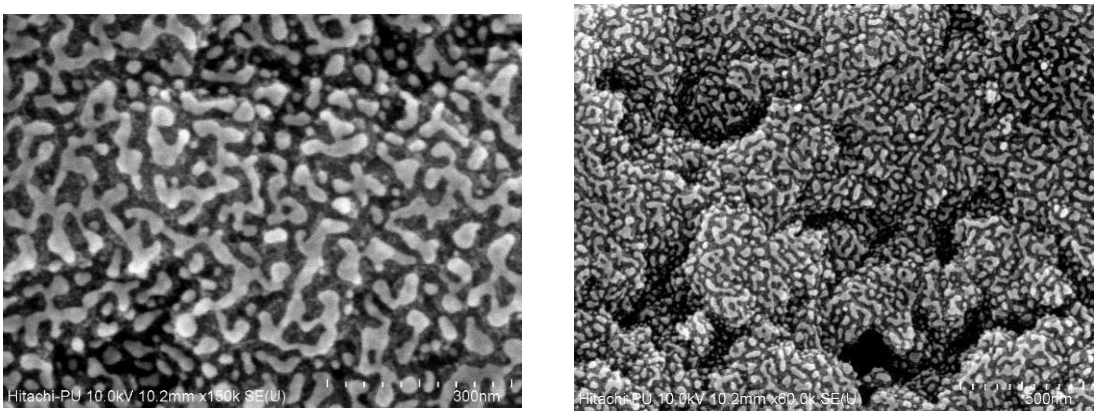

Figure 2. FESEM images of carbon-doped SnO_2 quantum dots showing agglomerated nanostructures.

Energy Dispersive Spectroscopy (EDS) and Elemental Mapping

Elemental composition and distribution of C-doped SnO2 QDs were studied by Energy Dispersive X-ray Spectroscopy (EDS) which was attached to the Hitachi, SU 8010 Series FESEM instrument. The Sn, O, and C was confirmed by the EDS analysis (Fig. 3), which shows that carbon was incorporated successfully. A uniform distribution of these elements by elemental mapping (Figure 4) indicates that the elements are not adsorbed on the surface but are uniformly doped.

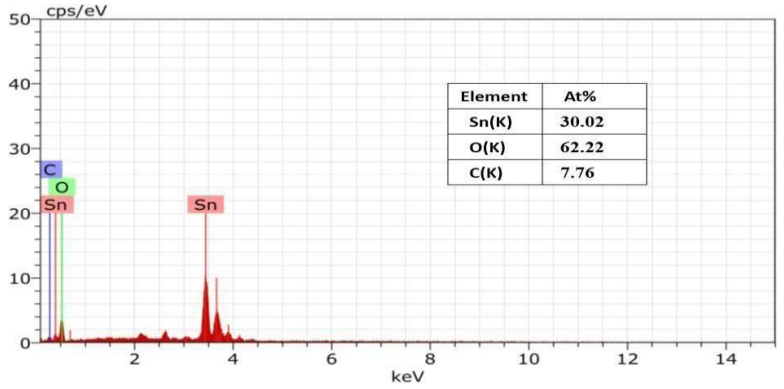

Figure 3. EDS spectrum of carbon-doped SnO_2 quantum dots confirming elemental composition.

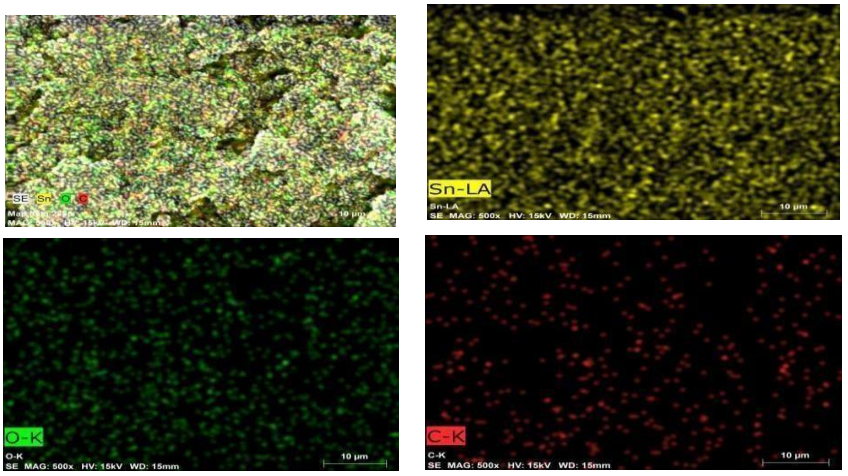

Figure 4. Images of elemental mapping with uniform distributions of Sn, O and C.

High Resolution Transmission electron microscopy (HRTEM) and Selected Area Electron Diffraction (SAED) Analysis

HRTEM and SAED pattern was recorded by JEOL, JEM-2100 Plus The almost spherical particles depicted by HRTEM images (Figure 5a-b) measure between 2.5 and 6 nm in size. The particle size distribution histogram (Figure 5c) provides the average size of 3.4 nm, which is in line with XRD results. The SAED patterns (Figure 5d) have concentric rings indexed to the (110), (101), (211) and (301) planes, which validates the polycrystalline character of the SnO_2 quantum dots.

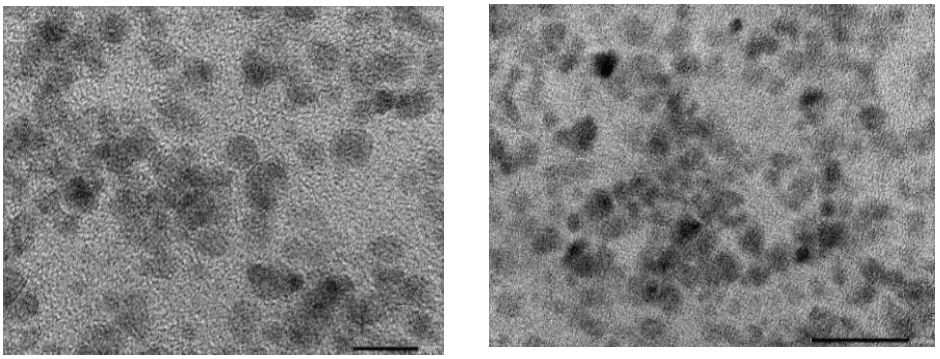

(a) **(b)**

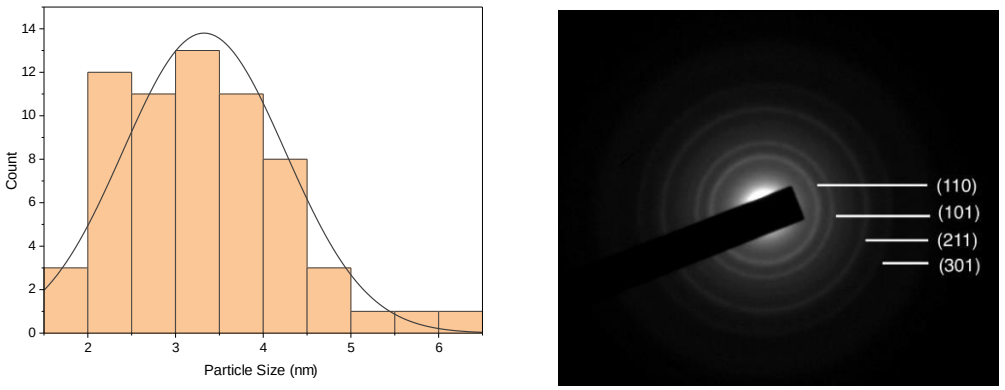

(a) **(d)**

Figure 5. (a–b) HRTEM images, (c) particle size distribution, and (d) SAED pattern.

FTIR Analysis

The structural vibrations of the prepared C-doped SnO_2 QDs were investigated by Fourier Transform Infrared (FTIR) Spectroscopy by Brucker, ALPHA II. FTIR spectrum indicates that there is a broad band at 3393 cm^{-1} (Fig. 6) which is related to the O-H stretching vibrations, signifying the presence of surface hydroxyl groups or adsorbed water. One band around 1630 cm^{-1} is ascribed to the bending vibrations of the water molecules. Typical Sn–O stretching bands can be found at the 700-300 cm^{-1} region and this indicates the presence of SnO_2. The band is at 600 cm^{-1} is attributed to the Sn–O–Sn stretching mode of the surface-bridging oxide. A band around 1040 cm^{-1} in metal oxide indicates presence of more than one oxygen atom attached to a single metal centre.

Other characteristics indicate that there are surface-bound functional groups that could be involved in a photocatalytic activity.

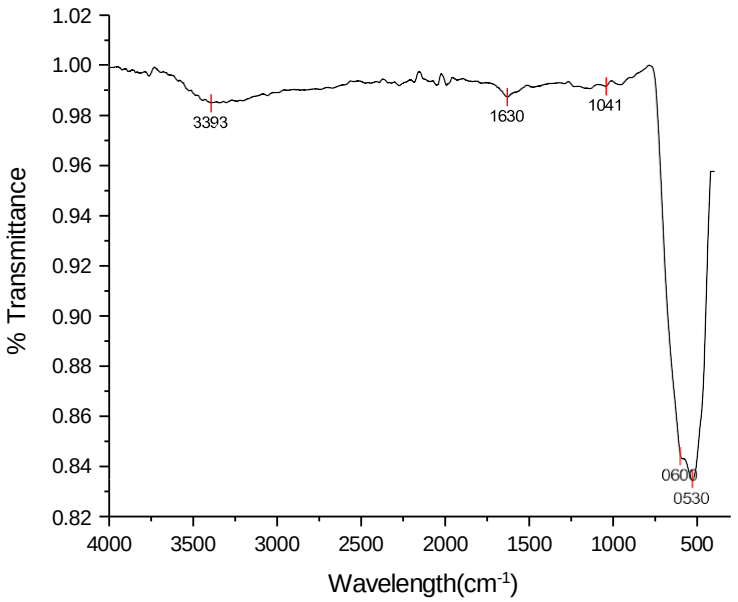

Figure 6. FTIR spectrum SnO_2 quantum dots after carbon doping with typical vibrational bands. Optical Properties (Band Gap Analysis)

The optical properties of the prepared were examined by Ultraviolet visible diffuse reflectance spectroscopy (UV-Vis-DRS) using Perkin Elmer, Lambda19 UV-VIS-NIR Spectrophotometer. The band gap energies were estimated using the Kubelka–Munk transformed Tauc plots. Since the semiconductor possesses a direct electronic transition, the $(F(R)h\nu)^2$ vs Energy(eV) plot was employed. Figure 7(a) presents the diffuse reflectance spectrum of carbon-doped SnO_2 quantum dots together with the inset Tauc plot. The extrapolation of the linear region of the plot to the photon energy axis yielded an optical band gap of approximately 3.3 eV.

Fig.7(b) further presents the diffuse reflectance spectrum of pure SnO_2 quantum dots together with the inset Tauc plot for optical band gap estimation. The extrapolated linear region yielded an optical band gap value of approximately 3.7 eV, which is higher than that observed for carbon-doped SnO_2 quantum dots. The band gap narrowing may be attributed to the formation of impurity energy levels and enhanced electronic interaction between the dopant and host lattice, which improves visible-light absorption and photocatalytic activity. The size of the crystallites in pure quantum dots is comparable to the Bohr radius, so it is expected that the bandgap energy will increase, due to quantum confinement effect (30-31). In the present investigation, it was found that the bandgap of SnO_2 QDs got reduced with the increase in the annealing temperature and further reduced in C-doped SnO_2 QDs(32). This is the reason for improved ability of C-doped SnO_2 QDs to absorb and photocatalyze in visible light as compared to pure SnO_2 QDs.

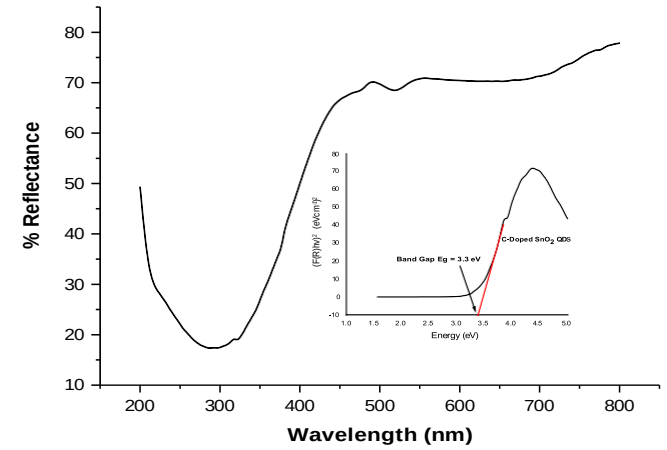

(a)

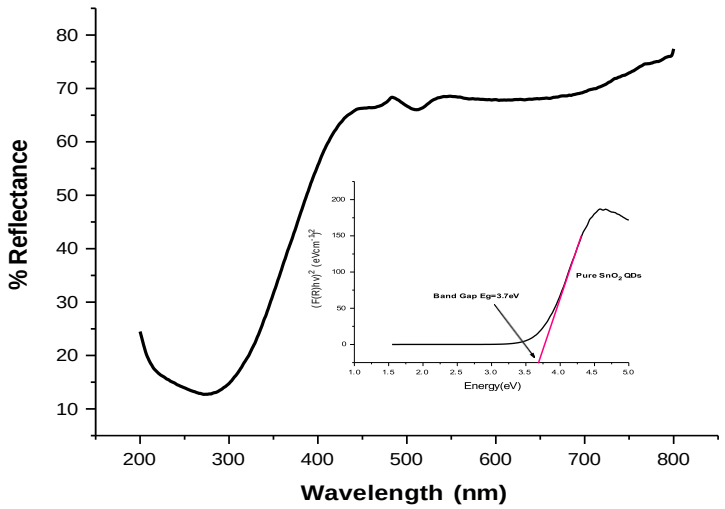

(b)

Figure 7. (a) DRS of carbon-doped SnO_2 QDs (b) undoped SnO_2 QDs together with the inset Tauc plot

Photocatalytic Degradation of Erythrosine

The photocatalytic activity of the catalyst was assessed by monitoring the degradation of Erythrosine dye (λmax = 527 nm). A stock solution of 1.0×10^{-3} M was prepared by dissolving the appropriate mass of Erythrosine in 100 mL of doubly distilled water; working solutions of the required concentration were prepared from this stock. Solution pH was adjusted using 0.1 N HCl and 0.1 N NaOH solutions. Irradiation was carried out using a 200 W tungsten lamp; light intensity was varied by adjusting the distance between the lamp and the reaction vessel. Aliquots were withdrawn at regular time intervals, and the absorbance was measured at 527 nm using a UV-Vis spectrophotometer. A plot of (2 + log A) against irradiation time was found to be linear for both C-doped SnO_2 QDs and pure SnO_2 QDs, confirming pseudo-first-order degradation kinetics. The apparent rate constant was determined from:

$$k = 2.303 \times Slope$$

The molecular structure of Erythrosine dye used in the study is shown in Figure 8.

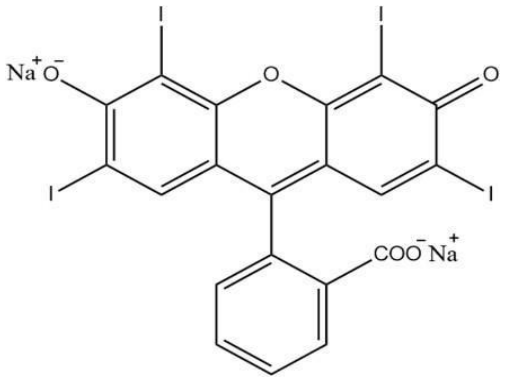

.

Figure 8. Molecular structure of Erythrosine dye.

A Typical Run: Comparative Study of C-doped and Pure SnO_2 QDs.

Carbon-doped SnO_2 was used in comparison with Pure(undoped) SnO_2 to determine the photocatalytic activity under the same conditions. The absorbance data are depicted by time (Table 1) and the degradation profiles (Figure 9) indicate that the doped sample has a quicker reduction in the dye concentration. The increased performance is a response to a better visible-light response and a more efficient charge carrier dynamics in the doped material, which justifies its increased photocatalytic efficiency in the investigated conditions.

Table 1: A Typical Run

pH = 7, (Erythrosine)=3.6x 10^{-6} M, C-Doped SnO_2=0.080gm, Light Intensity=60 $mWcm^{-2}$

Wavelength=527 nm	**C-Doped SnO_2 QD**		**Pure SnO_2 QD**	
Time(min.)	**Absorbance(A)**	**2+log A**	**Absorbance (A)**	**2+log A**
0	0.343	1.5352	0.343	1.5352
10	0.257	1.4099	0.302	1.48
20	0.22	1.3424	0.268	1.4281

30	0.181	1.2576	0.238	1.3765
40	0.142	1.1522	0.212	1.3263
50	0.115	1.0606	0.186	1.2695
60	0.093	0.9684	0.173	1.238
70	0.079	0.8976	0.163	1.2121
80	0.06	0.7781	0.14	1.1461
90	0.053	0.7242	0.121	1.0827
100	0.038	0.5797	0.102	1.0086
110	0.029	0.4623	0.091	0.959
120	0.025	0.3979	0.079	0.8976

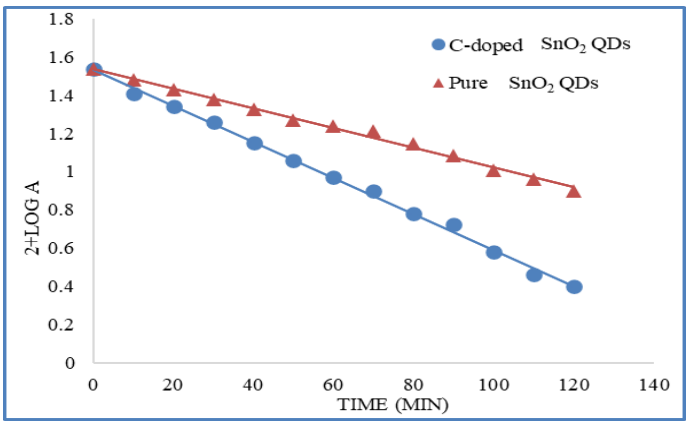

Rate constant — C-Doped SnO_2 QDs: $k = 3.61 \times 10^{-4}\ s^{-1}$

Pure SnO_2 QDs: $k = 1.98 \times 10^{-4}\ s^{-1}$

Fig. 9: A Typical Run Showing Comparative Degradation of Erythrosine by C-doped and Pure SnO_2 QDs (2 + log A vs. Time)

Effect of Parameters on Rate of Photocatalytic degradation

Effect of pH

The effect of pH on degradation was measured in the 5.5-8.5 range. The results are reported in table 2 and Figure 10. The rate constant rose with pH and peaked at a pH of about 7 and then decreased at higher pH. This tendency means that surface interactions and dye speciation contribute to the photocatalytic efficiency. The near-neutral pH conditions are favourable to efficient interaction between the dye and catalyst, and higher pH conditions can diminish efficacy because of electrostatic interactions and recombinations

Table 2: Effect of pH

[Erythrosine] = 3.6×10^{-6} M, C-doped SnO_2 QDs = 0.080 g, Light intensity= 60.0 $mWcm^{-2}$

pH	k × 10^4 (s^{-1})
5.5	1.35
6.0	1.51
6.5	2.97

7.0	3.61
7.5	2.36
8.0	2.05
8.5	1.34

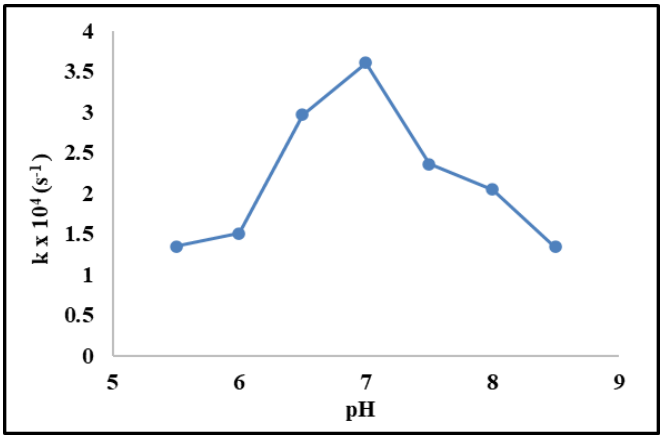

Figure 10. Effect of pH

Effect of Erythrosine Concentration

The effect of Erythrosine concentration was observed. The results are presented in table 3 and figure 11. The rate of degradation rose with the concentration of dye to an optimum level after which it declined. The first rise is due to the increased accessibility of dye molecules and the subsequent fall is tied to smaller light penetration and potential saturation of the catalyst on the surface. The observations show that there is an optimal concentration at which an optimum photocatalytic activity occurs.

Table 3: **Effect of Erythrosine concentration**

pH = 7.0, C-doped SnO_2 QDs = 0.080 g , Light intensity = 60.0 $mWcm^{-2}$

[Erythrosine] × 10^6 (M)	**k × 10^4 (s^{-1})**
2.8	2.93
3.6	3.61
4.4	3.45
5.2	3.11
6.0	2.57
6.8	2.51
7.6	2.48
8.4	2.23

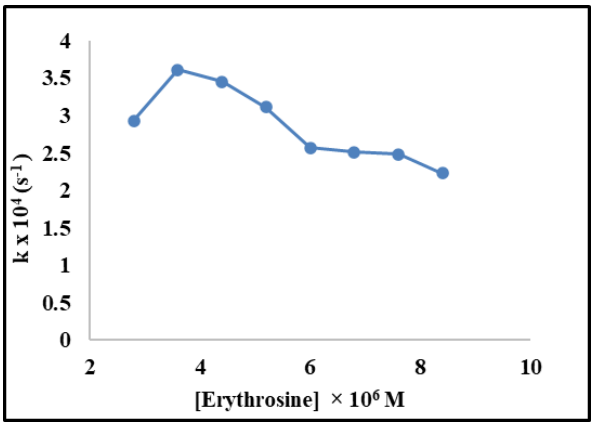

Figure 11. Effect of Erythrosine concentration

Effect of amount of C-doped SnO_2 QDs

The rate of degradation increased with amount of C-doped SnO_2 QDs until it reached a plateau at an amount of about 0.08 g shown in table 4 and figure 12. The growth at lower amount is an indication of the presence of more active sites and reactive species whereas further increase in amount of photocatalyst will only increase thickness of layers of the photocatalyst and not its exposed surface area.

Table 4: Effect of amount of C-doped SnO_2 QDs

***pH** = 7.0, [Erythrosine] = 3.6 × 10⁻⁶ M, Light intensity = 60.0 mWcm⁻²*

Amount of C-Doped SnO_2 QDs (g)	k × 10^4 (s^{-1})
0.02	1.37
0.04	1.49
0.06	2.88
0.08	3.61
0.10	3.16
0.12	3.30
0.14	3.22

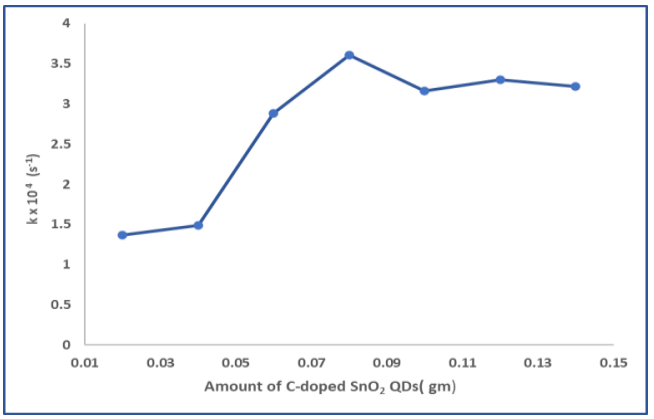

Figure 12. Effect of amount of C-doped SnO_2 QDs

Effect of Light Intensity

The rate of degradation was proportional to light intensity to an optimum behaviour, then a slight decrease with high intensities. The results of effect of intensity are tabulated in table 5 and presented in figure 13. Increased photon flux increases electron-hole pair production, though too much could cause recombination or non-productive energy loss, decreasing the overall efficiency.

Table 5: Effect of light intensity

pH = 7.0, [Erythrosine] = 3.6 × 10⁻⁶ M, C-doped SnO_2 QDs =0.080 g

Light Intensity ($mWcm^{-2}$)	$k \times 10^4$ (s^{-1})
20.0	1.05
30.0	1.42
40.0	2.26
50.0	2.49
60.0	3.61
70.0	3.25

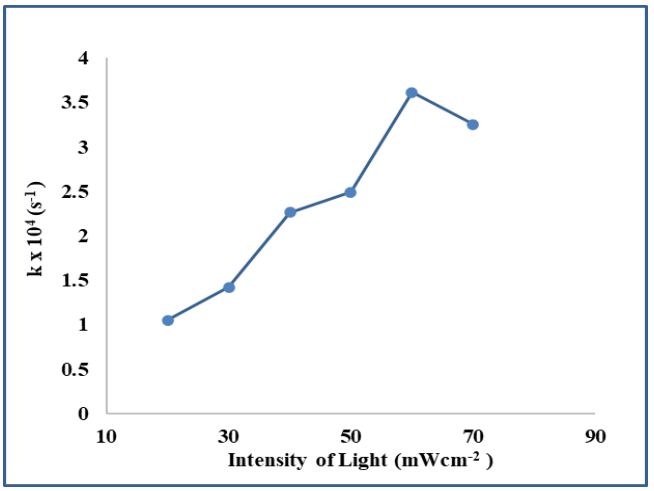

Figure 13. Effect of light intensity

Mechanism

In order to acquire an initial understanding of the degradation process, the influence of the hydroxyl radical scavenger 2-propanol was investigated. The addition of 2-propanol also led to a significant reduction in the rate of degradation of erythrosine than the control. This decrease means that hydroxyl radicals (· OH) are involved in the photocatalytic reaction.

On the basis of above experimental observations, a tentative mechanism is proposed for the photocatalytic degradation of Erythrosine using C-doped SnO_2 QDs semiconductor.

$$^1ETS_0 \xrightarrow{hv} {}^1ETS_1 \text{ (Singlet excited state)}$$

$$^1ETS_1 \xrightarrow{ISC} {}^3ETS_1 \text{ (Triplet excited state)}$$

$$SC \xrightarrow{hv} e^-(CB) + h^+(VB)$$

$$SC(h^+) + {}^-OH \longrightarrow {}^{\cdot}OH$$

$${}^{\cdot}OH + {}^3ETS_1 \longrightarrow \text{Product}$$

Where ETS= Erythrosine, SC=Semiconductor (C-doped SnO_2 QDs)

Erythrosine (ETS) absorbed appropriate radiation and excited to its first singlet excited state followed by intersystem crossing (ISC) to triplet state. Simultaneously, C-doped SnO_2 QDs also absorbed photons, to excite its electron from valence band to conduction band generated electron-hole pairs. This hole may abstract an electron from hydroxyl ions to generate hydroxyl radicals. These hydroxyl radicals then oxidize the dye molecules to products.

Conclusion

The present study conclusively demonstrates successful synthesis and characterization of carbon doped SnO_2 quantum dots by modified hydrothermal method. Structural and spectroscopic studies proved that the phase-pure tetragonal SnO_2 quantum dots with carbon incorporation in semiconductor matrix were successfully prepared with reduced optical bandgap. The photocatalytic degradation analysis conclusively assessed that C-doped SnO_2 quantum dots ($k = 3.61 \times 10^{-4}$ s^{-1}) function as highly effective visible-light-driven photocatalysts for the degradation of erythrosine. The carbon doping strategy substantially enhances photocatalytic performance relative to undoped SnO_2 quantum dots ($k = 1.98 \times 10^{-4}$ s^{-1}) by narrowing the effective optical bandgap, extending visible light absorption, and suppressing electron–hole recombination through the introduction of carbon-derived trap states. The photocatalytic degradation process adheres to pseudo-first-order kinetics, and the rate constant exhibits well-defined dependencies on solution pH, dye concentration, catalyst loading, and incident light intensity, all of which are in close accord with established mechanistic models for semiconductor-based heterogeneous photocatalysis. The scavenger study further corroborates the dominant role of hydroxyl radicals in the mineralization pathway of Erythrosine. Altogether, the results demonstrate the prospects of carbon-doped SnO_2 quantum dots in application of wastewater treatment with dye contaminants.

Acknowledgement

Author is thankful to SAIF, Panjab University Chandigarh for their support in the characterization of the photocatalyst through XRD, FESEM and EDX, HRTEM, XPS analysis, SICART, Anand for diffuse reflectance spectroscopy, and IIT, Indore for FT-IR analysis. Sincere thanks are also extended to Pacific Academy of Higher Education and Research (PAHER) University for providing the necessary technical and experimental support

References

1. Wang Z, Zhou Y, Xiao X, Liu A, Wang S, Preston RJS, Zaytseva YY, He G, Xiao W, Hennig B, Deng P. Inflammation and cardiometabolic diseases induced by persistent organic pollutants and nutritional interventions: Effects of multi-organ interactions. Environ Pollut. 2023;339:122756. https://doi.org/10.1016/j.envpol.2023.122756

2. Guo W, Pan B, Sakkiah S, Yavas G, Ge W, Zou W, Tong W, Hong H. Persistent Organic Pollutants in Food: Contamination Sources, Health Effects and Detection Methods. Int J Environ Res Public Health. 2019;16(22):4361. https://doi.org/10.3390/ijerph16224361

3. Chong MN, Jin B, Chow CWK, Saint C. Recent developments in photocatalytic water treatment technology: A review. Water Res. 2010;44(10):2997–3027. https://doi.org/10.1016/j.watres.2010.02.039

4. Pera-Titus M, García-Molina V, Baños MA, Giménez J, Esplugas S. Degradation of chlorophenols by means of advanced oxidation processes: A general review. Appl Catal B Environ. 2004;47(4):219–256. https://doi.org/10.1016/j.apcatb.2003.09.010

5. Ong CB, Ng LY, Mohammad AW. A review of ZnO nanoparticles as solar photocatalysts: synthesis,

mechanisms and applications. Renew Sustain Energy Rev.2018;81:536–551. https://doi.org/10.1016/j.rser.2017.08.020

6. Kant R. Textile dyeing industry an environmental hazard. Nat Sci. 2012;4(1):22–26. https://doi.org/10.4236/ns.2012.41004

7. Herrmann JM. Heterogeneous photocatalysis: fundamentals and applications to the removal of various types of aqueous pollutants. Catal Today. 1999;53(1):115–129. https://doi.org/10.1016/S0920-5861(99)00107-8

8. Saratale RG, Saratale GD, Chang JS, Govindwar SP. Bacterial decolorization and degradation of azo dyes: a review. J Taiwan Inst Chem Eng. 2011;42(1):138–157. https://doi.org/10.1016/j.jtice.2010.06.006

9. Crini G. Non-conventional low-cost adsorbents for dye removal: a review. Bioresour Technol. 2006;97(9):1061–1085. https://doi.org/10.1016/j.biortech.2005.05.001

10. Gupta VK, Suhas. Application of low-cost adsorbents for dye removal: a review. J Environ Manage. 2009;90(8):2313–2342. https://doi.org/10.1016/j.jenvman.2008.11.017

11. Ali H. Biodegradation of synthetic dyes: a review. Water Air Soil Pollut.2010;213:251–273. https://doi.org/10.1007/s11270-010-0382-4

12. Fujishima A, Zhang X, Tryk DA. TiO_2 photocatalysis and related surface phenomena. Surf Sci Rep. 2008;63(12):515–582. https://doi.org/10.1016/j.surfrep.2008.10.001

13. Hoffmann MR, Martin ST, Choi W, Bahnemann DW. Environmental applications of semiconductor photocatalysis. Chem Rev. 1995;95(1):69–96. https://doi.org/10.1021/cr00033a004

14. Elmolla ES, Chaudhuri M. Comparison of different advanced oxidation processes for treatment of antibiotic aqueous solution. Desalination. 2010;256(1–3):43–47. https://doi.org/10.1016/j.desal.2010.02.019

15. Asahi R, Morikawa T, Ohwaki T, Aoki K, Taga Y. Visible-light photocatalysis in nitrogen-doped titanium oxides. Science. 2001;293(5528):269–271. https://doi.org/10.1126/science.1061051

16. Chen X, Mao SS. Titanium dioxide nanomaterials: synthesis, properties, modifications, and applications. Chem Rev. 2007;107(7):2891–2959. https://doi.org/10.1021/cr0500535

17. Schneider J, Matsuoka M, Takeuchi M, Zhang J, Horiuchi Y, Anpo M, Bahnemann DW. Understanding TiO_2 photocatalysis: mechanisms and materials. Chem Rev. 2014;114(19):9919–9986. https://doi.org/10.1021/cr5001892

18. Sakthivel S, Kisch H. Daylight photocatalysis by carbon-modified titanium dioxide. Angew Chem Int Ed Engl. 2003;42(40):4908–4911. https://doi.org/10.1002/anie.200351577

19. Jassby D, Farner Budarz J, Wiesner M. Impact of aggregate size and structure on the photocatalytic properties of TiO_2 and ZnO nanoparticles. Environ Sci Technol. 2012;46(13):6934–6941. https://doi.org/10.1021/es202009h

20. Brus LE. Electron–electron and electron-hole interactions in small semiconductor crystallites: the size dependence of the lowest excited electronic state. J Chem Phys. 1984;80(9):4403–4409. https://doi.org/10.1063/1.447218

21. Alivisatos AP. Semiconductor clusters, nanocrystals, and quantum dots. Science. 1996;271(5251):933–937. https://doi.org/10.1126/science.271.5251.933

22. Di Valentin C, Pacchioni G, Selloni A. Theory of carbon doping of titanium dioxide. Chem Mater. 2005;17(26):6656–6665. https://doi.org/10.1021/cm051921h

23. Chen X, Liu L, Yu PY, Mao SS. Increasing solar absorption for photocatalysis with black hydrogenated titanium dioxide nanocrystals. Science. 2011;331(6018):746–750. https://doi.org/10.1126/science.1200448

24. Liu G, Wang L, Yang HG, Cheng HM, Lu GQ. Titania-based photocatalysts: crystal growth, doping and heterostructuring. J Mater Chem. 2010;20(5):831–843. https://doi.org/10.1039/B909930A

25. makrishnappa S,Lakshmipathi GD. Photocatalytic activity of C, N and S doped SnO_2: effective band gap engineering to increase the quantum efficiency and exploration of the change in the position of Fermi energy with dopant concentration and its influence on photoreactivity. Pure Appl Chem. 2025;97(12). https://doi.org/10.1515/pac-2024-0332

26. Pan X, Yang MQ, Fu X, Zhang N, Xu YJ. Defective TiO_2 with oxygen vacancies: synthesis, properties and photocatalytic applications. Nanoscale. 2013;5(9):3601–3614. https://doi.org/10.1039/C3NR00476G

27. Batzill M, Diebold U. The surface and materials science of tin oxide. Prog Surf Sci. 2005;79(2–4):47–154. https://doi.org/10.1016/j.progsurf.2005.09.002

28. Reddy BM, Reddy GK, Ganesh I, Ferreira JMF. Cr-doped SnO_2 quantum dots: synthesis, characterization, and enhanced photocatalytic activity under visible light irradiation. Ceram Int. 2017;43(2):2750–2759. Available

from https://doi.org/10.1016/j.mseb.2017.06.007

29. Tirado-Guízar A, Pina-Luis GE, Paraguay-Delgado F. Ecofriendly synthesis of ultra-small metal-doped SnO_2 quantum dots. MRS Communications. 2015;5(1):63–69. https://doi.org/10.1557/mrc.2015.11

30. Ahmed F, Arshi N, Anwar MS, Danish R, Koo BH. Quantum-confinement induced enhancement in photocatalytic properties of iron oxide nanoparticles prepared by ionic liquid. Ceramics International. 2014;40(10):15743–15751 https://doi.org/10.1016/j.ceramint.2014.07.098

31. Wang C, Thompson RL, Ohodnicki P, Baltrus J, Matranga C. Size-dependent photocatalytic reduction of CO_2 with PbS quantum dot sensitized TiO_2 heterostructured photocatalysts. Journal of Materials Chemistry. 2011;21(35):13452–13457 https://doi.org/10.1039/C1JM12367J

32. Babu B, Reddy IN, Yoo K, Kim D, Shim J. Bandgap tuning and XPS study of SnO_2 quantum dots. Materials Letters. 2018;221:211-215. https://doi.org/10.1016/j.matlet.2018.03.107